Low-Temperature (70 °C) Ambient Air Plasma-Fabrication of Inkjet-Printed Mesoporous TiO₂ Flexible Photoanodes

AUTHOR'S PRE-PRINT v 1.2 (29.8.2017)

Tomáš Homola[*a], Masoud Shekargoftar [a], Petr Dzik [b], Richard Krumpolec [a], Zuzana Ďurašová [b], Michal Veselý [b], Mirko Černák [a]

[a] R&D Center for Low-Cost Plasma and Nanotechnology Surface Modifications (CEPLANT), Department of Physical Electronics, Faculty of Science, Masaryk University, Kotlářská 267/2, 611 37 Brno, Czech Republic

[b] Faculty of Chemistry, Brno University of Technology, Purkyňova 118, 612 00 Brno, Czech Republic

*Corresponding author: tomas.homola@mail.muni.cz, Tel: +420 549 49 4974
ORCID: Tomáš Homola: 0000-0002-8522-6169

ABSTRACT: Titania/silica electron-generating and -transporting nanocomposite 300-nm layers of high porosity were deposited onto ITO/PET flexible foils using inkjet printing. Prior to printing, the ITO surface had been modified by novel low-temperature ambient air roll-to-roll plasma in order to enhance its surface properties by removing carbon and oxygen contaminants, a process that led to rapid improvement of surface energy. Consequently the ITO work function, an important parameter involving charge injection efficiency in energy harvesting systems, increased by 1 eV. Afterwards, the TiO₂/methyl-silica ink exhibited excellent wetting on a 2-s plasma-treated ITO surface. The coating was further processed/mineralized by an additional low-temperature ambient air plasma treatment step. The plasma processing of raw photoanodes led to the mineralization of the methyl-silica binder which resulted in the formation of a fully inorganic TiO₂/SiO₂ mesoporous structure and significantly increased electrophotocatalytic activity, leading to increased photocurrents. The entire two-step plasma process was performed at low-temperature (70 °C) and high speeds, enabling practical applications of such a procedure for large-area fabrication of flexible photoanodes.

KEYWORDS: plasma treatment; ambient air plasma; TiO₂ flexible photoanode; mesoporous coating; roll-to-roll processing; inkjet printing

1. Introduction

Flexible and printed electronics [1,2] have attracted increased attention in recent times because of their potential to enable low-cost and high-throughput manufacturing of electronics on cheap plastic substrates for various applications, including rollable and foldable displays, smart packaging, photovoltaics, and more. Printed photovoltaics could contribute greatly to increasing global access to cheap energy. Dye-sensitized solar cells (DSSC) [3–6] and perovskite solar cells [7–10], in which the photo-electrochemical system relies upon a mesoporous TiO_2 layer, have emerged as a promising low-cost photovoltaic technology and constitute a notable application field for semiconducting photoanodes. Other suitable applications for photoanodes involve, for example, photocatalytic treatment of water [11,12], hydrogen production [13,14], energy storage [15] and various sensing systems.

Titanium dioxide (TiO_2) photoelectroactive layers have already been deposited by a range of techniques both in gas and liquid phases. Deposition from liquid is popular, since the manufacturing equipment is relatively simple and often compatible with ambient conditions. Recently, Wang et al. employed yttrium-nitrogen co-doped sol-gel mesoporous TiO_2 in DSSC of 5.4% power conversion efficiency [16], and Giordano et al. used lithium-doped mesoporous TiO_2 as an efficient photoanode in a perovskite solar cell of 19% power conversion efficiency with negligible hysteretic behaviour [17]. The reduction of energy costs is crucial to flexible photovoltaics [8], something that can be achieved either by increasing the efficiency of devices or by reducing manufacturing expenditure by means of various atmospheric-pressure fast-fabrication methods such as spraying [18], screen-printing [19], gravure printing [20] and inkjet printing [5,21,22] as well as other printing techniques [23], e.g. blade coating [24] and slot die coating. Numerous works in which TiO_2 mesoporous layers have been employed in photovoltaics report the use of coating formulations that have to be either *i)* thermally sintered at temperatures higher than 150 °C [25] or *ii)* low-temperature sintered (UV and/or plasma) for quite some time (more than 30 min) [26,27]. However, high temperatures preclude the use of such fabrication procedures for thermally sensitive substrates [28], such as flexible plastics, as most thermo-plastics limit the treatment temperature to around 150 °C [3]. In particular, the deposition of TiO_2 photoanodes on PET/PEN foils with significant potential for printed electronics applications has emerged as a considerable challenge. For example, A. Yasin et al. recently developed aqueous screen-printable paste for fabrication of mesoporous anatase-rutile TiO_2 film for DSSC application [29]. The mesoporous structure was achieved by high-temperature (400 °C) sintering for 30 min, during which polyethylene glycol evaporated from the paste and facilitated increased porosity. R. Li et al. modified mesoporous TiO_2 photoanodes with an Al-doped TiO_2 layer [30]. High-temperature sintering at 500 °C for 30 min was applied after both depositions. Other recently published works also refer to high-temperature (>150 °C) plasma

sintering methods [31,32]. However, slow, low-temperature curing, employing UV or remote plasmas involves problems when fast/low-cost roll-to-roll manufacturing is envisaged. Further, the use of low-pressure plasma treatment of mesoporous TiO_2 [33,34] is currently therefore inconvenient for low-cost production because it is relatively slow and requires complex vacuum systems.

Low-temperature atmospheric plasma treatments have thus become very important to research into low-cost production of photovoltaics [35]. Very recently, Lisco et al. [36] used an He/O_2 (3 slm/15 sccm respectively) dielectric barrier discharge plasma jet (14.16 kHz, 10 kV, 10 W) in order to pre-treat fluorine-doped tin oxide (FTO) glasses prior to cadmium sulphide (CdS) sonochemical deposition for photovoltaic application. The plasma treatment for 40 s (treated area 5 cm^2) led to an effective removal of adventitious carbon from 31 at.% to 10 at.%. This plasma pre-treatment significantly increased the CdS grain size, and also resulted in higher uniformity and quality of film. The effect of plasma was also confirmed for flexible substrates: flexible glass, stainless steel (200 μm) and polyimide (50 μm) [37].

High-speed and low-cost manufacturing across large areas can be achieved using roll-to-roll processing [38,39]. In previous work [40] the authors reported on a fast (approx. 1 min), low-temperature (70 °C) plasma mineralization process that led to energy-efficient manufacturing of TiO_2 mesoporous photoanodes deposited by inkjet printing on FTO glass. The ambient-air, high-energy-density plasma was generated by dielectric barrier discharge in a coplanar arrangement of electrodes; the diffuse coplanar surface barrier discharge (DCSBD) led to mineralization of a methyl-silica binder and transformation of the water-soluble coating into a TiO_2/SiO_2 hybrid nanocomposite. Low-temperature ambient air DCSBD plasma has also been tested for fast calcination of metalorganic CeO_2 [41] and Al_2O_3 [42,43] nanofibers. The distance between treated material and DCSBD ceramic is crucial and the most effective treatment was found at a distance of approx. 0.3 mm [44]. DCSBD plasma treatment of non-porous dielectric materials is often associated with difficulties related to electrostatic charges generated on the material surface leading to attraction of the treated material towards the plasma and consequently to contact of the treated material with DCSBD ceramic. Thus the ambient-air gap between the treated material and the DCSBD ceramic has a tendency to shrink to zero, leading to plasma extinction. As a solution of this problem, the authors have developed a pilot roll-to-roll plasma treatment apparatus with concavely-curved ceramic DCSBD electrodes.

In this study, high-energy-density diffuse homogenous surface plasma generated by curved DCSBD in ambient air was employed for *i)* pre-treatment of a flexible ITO surface in order to increase its surface energy and obtain excellent wetting of mesoporous titania/methyl-silica films. Subsequently, the plasma treater was used for *ii)* mineralization of titania/methyl-silica films to titania/silica hybrid nanocomposite

functional coating on flexible ITO/PET foils. A range of experimental techniques were employed to study the plasma pre-treatment of ITO and to monitor methyl-silica mineralization. The results obtained indicate that the upgraded DCSBD technique enables fast (~ 1 min) fabrication of flexible TiO_2 photoanodes on ITO/PET foil in ambient air at low temperature (70 °C) in conditions closely akin to continuous roll-to-roll manufacturing.

2. Experimental

Indium tin oxide (ITO)-coated polyethylene terephthalate (PET) (Sigma Aldrich, product No. 639303), of surface resistivity 60 Ω/sq and total thickness 127 μm, was used a flexible substrate. The mesoporous titania/methyl silica film was deposited using an experimental Fujifilm Dimatix 2831 inkjet printer. An ink denoted as 10AD was prepared by mixing 6 mL of titania dispersion (20 wt% of nanoparticulate titania Evonik P25 in Dowanol PM solvent) with 2 mL of a recently-reported organosilica binder [45] (20 wt% in anhydrous ethanol) and 8 mL of isobutanol. Approx. 2 cm^3 of 1-mm glass balls were added to this in a 20-mL glass vial and this was placed overnight on an oscillating shaker set to 1000 rpm. Thus, the titania/binder ratio was 75:25 and the thickness of the coating was approx. 300 nm. The materials and procedures employed for the printable suspension formulation have been reported in detail in our previous work [40].

The atmospheric-pressure ambient air plasma was generated by dielectric barrier discharge (DBD) with electrodes of curved-coplanar configuration: diffuse coplanar surface barrier discharge (DCSBD), manufactured by Roplass, Czech Rep. The DCSBD plasma unit, at a curvature of 1/14.8 cm^{-1}, generates homogeneous large-area (20 × 8 cm^2) high-power-density (400 W/160 cm^2, i.e. 2.5 W/cm^2) surface plasma in ambient air. The plasma unit was located in close vicinity to a surface of treated ITO/PET that was fixed on a dielectric roller with a diameter of 14.8 cm and a circumference of 92.95 cm. A huge decrease in power was observed during the ITO surface treatment; this appears in Supplementary **Figure S1** and is further discussed in the Supplementary Material. The distance between the plasma unit and surface of the treated sample was approximately 0.3 mm and may be varied with precision at 0.05-mm steps. The speed of the roller and corresponding treatment time (effective plasma width 8 cm) varied between 18.6 – 4.1 $cm.s^{-1}$ and 0.25 s – 2s. Plasma treatments taking longer than 2 s were achieved by multiple passes of the sample through the plasma. The plasma system was used for both *i)* cleaning and activation of the ITO/PET flexible substrate and *ii)* low-temperature mineralization of TiO_2 mesoporous films. Whereas the cleaning and activation of ITO/PET was investigated with treatment times ranging from 0.25 s – 8 s, the mineralization of TiO_2 films was performed with treatment times ranging from 2 – 64 s. The plasma cleaning and activation of ITO/PET, printing of titania/methyl-silica films and mineralization of titania/methyl-silica films were

completed in three independent steps, i.e. the process was not fully integrated in a roll-to-roll line. The delays were approximately an hour. The process of plasma mineralization of flexible TiO_2 films using novel curved DCSBD plasma is visualized in Figure 1.
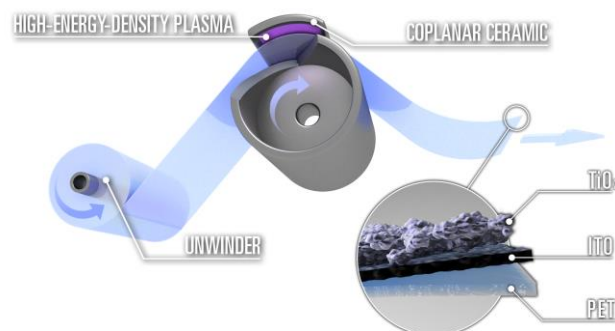

Figure 1. Visualization of plasma mineralization process of TiO_2 mesoporous flexible photoanodes.

The surface properties of the plasma-treated ITO surface were investigated by means of sessile droplet (2-μL) contact-angle measurements of demineralized water, ethylene glycol, diodomethane and formamide using SeeSystem (Advex Instrument, Czech Rep.) In total, eight measurements per sample and four different samples were used to calculate the free surface energy of the ITO surface, using the Owens-Wendt model [46]. Further, the total surface tension of the ink used for printing was determined by the Du Noüy ring method performed with Sigma 701 force tensiometers (Dyne Testing, UK) and its dispersive component was determined by analysing the contact angle on a teflon surface. The durability of the plasma treatment was investigated at a range of 15 min to 72 hours after plasma treatment. The samples were stored under ambient air (approx. 24 °C and 60 % relative humidity). The ITO surface was further investigated by X-ray photoelectron spectroscopy (XPS) using an Al Kα ESCALAB 250Xi apparatus (ThermoFisher Scientific). All samples were measured at two spots (650 μm) at a takeoff angle of 90° in 10^{-8} mbar vacuum at 20 °C. An electron flood-gun was used to compensate for charges on sample surfaces. The spectra were referenced to C 1s at 284.8 eV. UPS was acquired by Kratos Supra under normal emission using He I (21.22 eV) as the excitation source with a pass energy of 5 eV. A sample bias of −9 eV, in order clearly to observe the secondary electron cutoff, and an electron flood gun was employed for charge compensation. A Ntegra Prima (NT-MDT) atomic force microscope (AFM) was used to measure the morphology of ITO surfaces. The root mean square (RMS) roughness was calculated from two different 2 × 2-μm scans taken in semi-contact mode.

The titania/methyl silica films were deposited on plasma pre-treated ITO/PET flexible substrates. The quality of the printed films was inspected by means of microphotographs taken with an Nikon Eclipse E200 microscope equipped with a Nikon D5000 digital camera. The variability in printing quality was related to surface energy and expressed by means of wetting envelope diagrams, which conveniently illustrate the degree of wetting of the surface investigated [47]. The

electrochemical properties of the plasma-mineralized titania/methyl silica films were characterized by linear sweep voltammetry and chronoamperometry. The measured photocurrents proved an effective tool for the investigation of the binder state and its transformation from methyl-silica to silica. Direct measurements and characterization of the mineralization using FTIR and XPS have been reported in Homola et al. [40].

Photoelectrochemical characterization was performed by linear sweep voltammetry at room temperature using a two-terminal setup. The measured cells consisted of separate 1-cm^2 titania photoanodes and cathodes made of strips of stainless-steel sheet. The sample cell was fitted into a custom-built quartz cuvette filled with 0.1 M perchloric acid (35 mL) and placed on an optical bench equipped with a fluorescent UV-A lamp emitting a broad peak centred at 365 (Sylvania Lynx-L, 11 W). A magnetic stirrer was placed beneath the cuvette and a magnetic flea within provided efficient electrolyte mixing. The lamp emission was monitored by a Gigahertz Optic X97 irradiance meter with a UV-3701 probe with the irradiance set to 2 mW/cm^2 by adjusting the lamp-to-cuvette distance. Current potential and current-time measurements were taken with a custom computer-controlled power source meter built on the basis of the National Instruments Labview platform (NI cDAQ-9172 interface with NI9219 and NI9263 convertors), supplying linear voltage sweeps and measuring currents down to the sub-μA range.

3. Results and discussion

3.1. ITO surface chemistry.

Figures 2a and **2b** present the evolution of elements on ITO surfaces after plasma treatment for 0.25 – 8 s. The reference ITO surface showed a high amount of carbon at 53.4 at.%, 32.8 at.% of oxygen, 11.3 at.% of indium, 1.4 at.% of tin and approx. 1.1 at.% of nitrogen. The C/O and In/Sn ratios were 1.6 and 7.9. The plasma treatment of the ITO surface clearly had a swift and significant effect on carbon concentrations, which decreased exponentially, in similar fashion to the water contact angle reported in **Figure S2**. Since plasma treatment led to a progressive etching of carbon contaminants, concentrations of oxygen and indium increased. The lowest reported value of carbon contamination was found at 12.9 at.% after plasma treatment for 8 s. The oxygen and indium atomic concentrations after plasma treatment for 8 s were 48.1% and 27.4% respectively. The plasma clearly led to cleansing the ITO surface of carbon and the C/O ratio decreased from 1.6 for an untreated sample to 0.3 for a sample treated for 8 s, as appears in **Table 1**. The bonding between carbon and oxygen was further studied by analysing XPS C1s high-resolution peaks, presented in **Figure S3.** An increase in C–O and C=O bonds indicated oxidations related to relative decreases in C–C and C–H. Thus effective ITO etching from hydrocarbons parallels decreases in C/O ratio.
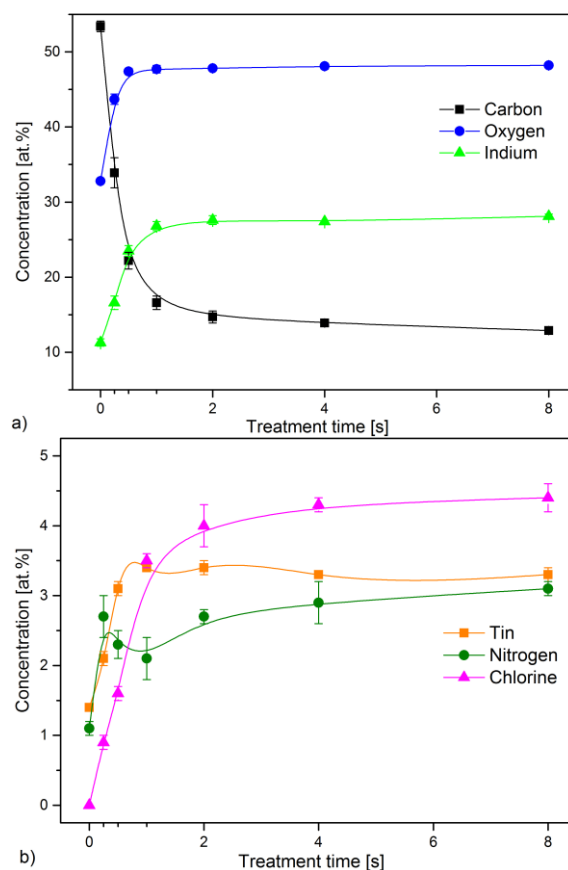

Figure 2. Evolution of elements a) C, O, In; b) Sn, N, Cl on ITO surfaces treated in plasma for 0.25 – 8 s.

The plasma treatment of ITO also led to a significant increase of tin, which reached a maximum of 3.4 at. % after plasma treatment for 1 s. Longer treatments had no effect on the concentration of tin. The In/Sn ratio (**Table 1**) of untreated ITO was 7.9 and remained fairly constant for treatment times ranging between 0.25 s and 1 s. For longer treatments, the In/Sn ratio increased slightly, reaching 8.4 for 8-s treatment. The plasma treatment also led to an increase in the atomic concentration of nitrogen, from 1.1% for an untreated sample to 3.1% for a sample treated in plasma for 8 s. The ITO surface treatment resulted in a significant concentration of chlorine, logarithmically increasing with treatment time and reaching 4.4 at. %. Since chlorine is often added to the ITO surface to increase the work function [48], plasma treatment had a positive effect on such ITO-electrode surface conditions.

ITO surface	C/O	In/Sn	O/In	WF
Untreated	1.6	7.9	2.9	3.8 eV
0.25-s treated	0.8	7.8	2.6	4.3 eV
2-s treated	0.3	8.2	1.7	4.9 eV
8-s treated	0.3	8.4	1.7	4.9 eV

Table 1. Stoichiometry and work function (WF) of ITO treated in plasma for 0.25 s, 2 s and 8 s.

Table 1 also shows the stoichiometry of indium oxide In_2O_3. Since approx. 90% of ITO should be in the form of indium oxide, the O/In ratio was expected to be 1.5. The values presented in **Table 1** clearly show that O/In was two times higher for untreated ITO, which also indicates oxygen

contaminants on ITO surfaces. Although the overall atomic concentration of oxygen **(Figure 2a)** increased after plasma treatment, O/In decreased significantly after it and reached 1.7 after plasma treatment for 2 s. Longer plasma treatment had no further effect on the O/In ratio, which remained at 1.7 and close to anticipated In_2O_3 stoichiometry. The O1s XPS high-resolution peak was further analyzed after work [49]. O1s comprises three main components related to lattice oxygen in In_2O_3, which appears at the lowest binding energies, around 530.5 eV; impurities containing oxygen appearing at the highest binding energies, around 532.5 eV; and amorphous oxygen as $In(OH)_3$ or InOOH lies between lattice and impurity oxygen in energy terms. The O1s peak appears in **Figure 3** and shows that plasma treatment led to a decrease in the peak related to oxygen impurities, whereas the peak related to lattice oxygen rose significantly. The change in amorphous oxygen component is not made clear in **Figure 3;** however according to Homola et al. [49] such change may be related to formation of polar $In(OH)_3$ or InOOH that might render the energy on the ITO surfaces higher. Analysis of O/In stoichiometry together with O1s peak demonstrated that plasma treatment had a significant effect on removal of oxygen impurities. These results indicate that decrease in oxygen was related to the form of oxygen impurities. The high-resolution peak presented in **Figure S4** shows that In3d spectra were shifted towards higher binding energy, which can be explained by oxidation and further supports the increased oxygen presented in **Figure 2a** and formation of polar groups suggested by work [49].
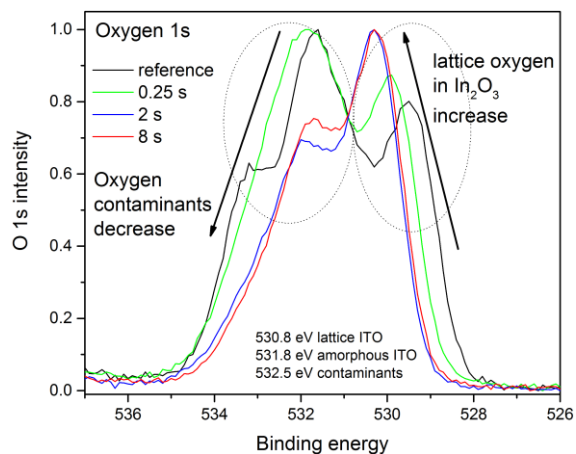

Figure 3. O1s peak showing decreased oxygen in contaminants and increased concentration of oxygen in In_2O_3 lattice for ITO surfaces treated in plasma for 0.25 s, 2 s and 8 s.

3.2. ITO surface energy.

The changes in surface chemistry induced by plasma treatment led to significant improvements of the surface energy. **Figure 4a** shows the evolution of the free surface energy of ITO surfaces with plasma treatment ranging from 0.25 s to 8 s. The surface energy of the untreated ITO surface was approx. 31.5 mJ/m^2 and plasma treatment for a very short time (0.25 s) led to a significant rise to 54.6 mJ/m^2, which is a 73% increase. After plasma treatment for 2 s, ITO exhibited a surface energy of approx. 64.0 mJ/m2,

corresponding to a 104% increase. Prolonging plasma treatment time led to slightly higher values for surface energy. The surface energy was calculated from contact angles of various liquids and the all measured contact angle values are summarized in **Table S1 a – d** in supplementary material. The evolution of water contact angle is often an interesting parameter; however, it describes only the polar part of the surface energy. The water contact angle (**Figure S2)** of untreated ITO surface was approx. 72° and decreased to 43° and 15° after plasma treatment for 0.25 and 2 s respectively. The importance of polar and dispersive parts of surface energy is discussed later.

The surface changes induced by atmospheric plasma were not permanent and the surface had a tendency to revert towards its original conditions before plasma treatment. The surface energy changes after plasma treatment were monitored for up to 96 hours for various treatment times. **Figure 4b** shows surface energy as a function of ageing time for ITO surfaces treated in plasma for 0.25 s, 2 s and 8 s. The decrease in surface energy was very swift, e.g. a sample treated for 0.25 s showed surface energy 49.7 mJ/m^2 after being exposed to ambient air for only 15 min. Subsequent decrease was quite slow and saturation was found at 44.21 mJ/m^2 for a surface exposed to ambient air for 96 hours. This was still, however, a significantly higher value of surface energy than an untreated ITO surface, of which the surface energy was approx. 31.5 mJ/m^2. The samples treated in plasma for longer periods of time, e.g. 2 s and 8 s, showed similar decrease characters, but since plasma treatment for longer periods of time yielded higher surface energy, the saturation after 96 hours was found at 48.7 mJ/m^2 at 2 s and 51.5 mJ/m^2 at 8 s.
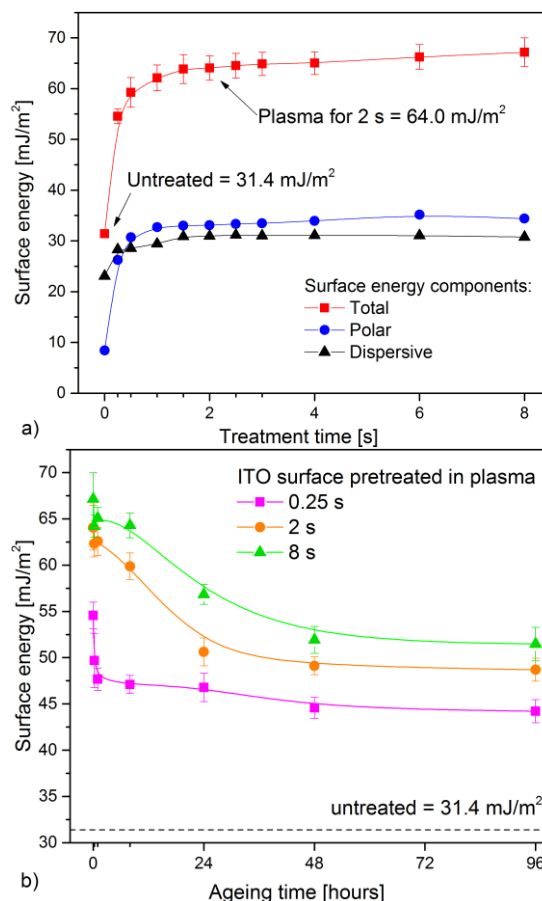
Figure 4. Surface energy of ITO a) pre-treated in plasma for 0.25 – 8 s and b) pre-treated in plasma for various times (0.25 s, 2 s, and 8 s) and stored under ambient conditions for 0.15 – 96 hours.

The ageing effects after plasma treatment have been described by others [50,51]. They are related to attachment of carbon contaminants from ambient air and deterioration of hydrophilic polar groups. The ageing rate is crucial to the methodology of inkjet printing of TiO_2 mesoporous coating; i.e. whether the inkjet printing should be carried out immediately after the plasma treatment, or whether a delay is acceptable. Because the ageing effect led to saturation of surface energy that was still significantly higher than an untreated surface, a delay between individual steps is acceptable and permits the use of plasma pre-treatment in non-continuous fashion as well, i.e. the ITO/PET roll can be modified by plasma and then transported to a roll-to-roll inkjet printer. In this mode, the delay between plasma treatment and inkjet printing was around an hour, thus the surface energy of ITO at printing was always slightly lower than reported immediately after treatment.

3.3. ITO work function.

Work function is defined as the minimum energy required to remove an electron from the Fermi level of the electrode to the vacuum level [52]. **Figure 5** presents the UPS spectra of ITO surfaces treated in air plasma for various times. The secondary cutoff shift indicates a significant increase in work function for plasma-treated ITO surfaces, as summarized in **Table 1**. The untreated ITO surface showed a work function of 3.8 eV and even very short exposure to plasma led to a significant increase, to 4.3 eV. Longer plasma treatment, for 2 s and 8 s, increased work function to 4.9 and 4.9 eV respectively. It is apparent that an increase in work function may be clearly associated with carbon contamination removal and improvement of O/In stoichiometry. Furthermore, the increase in work function may be related to the plasma deposition of strongly electronegative oxygen polar functional groups [53]. Additionally, the increase in chlorine concentration, as detected by XPS, could also contribute to higher surface electronegativity and thus increase work function. First-principle calculations based on density functional theory (*ab initio*/DFT) suggest that decreasing the surface methyl coverage on transparent conductive oxides leads to an increase in work function, which is explained as a result of an electronegative surface and associated reinforcement of the original surface dipole moment [54,55]. However, the significance between chlorine and oxygen polar groups on ITO work function remains unclear.
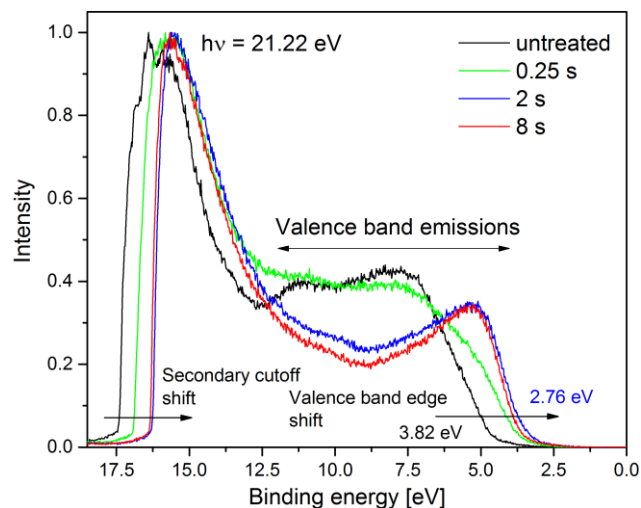
Figure 5. UPS spectra of ITO surfaces treated by plasma for 0.25 s, 2 s and 8 s.

3.4. ITO surface morphology

AFM scans of untreated ITO surfaces appear in **Figure 6a** with the calculated RMS roughness embedded within the images. The untreated ITO surface is of crystalline structure with an average grain size of about 40 nm and RMS roughness of 1.35 nm. The plasma treatment had no significant effect on the ITO surface, as is apparent from **Figures 6 b – d**; the size and distribution of the grains remained unaffected. However, the overall roughness decreased with time after plasma treatment and reached 0.74 nm after 8 s. The plasma treatment evidently had a minor smoothing effect, which could be explained in similar fashion to the results above: by the decrease of carbon contaminants while the structure of the ITO remained undamaged.
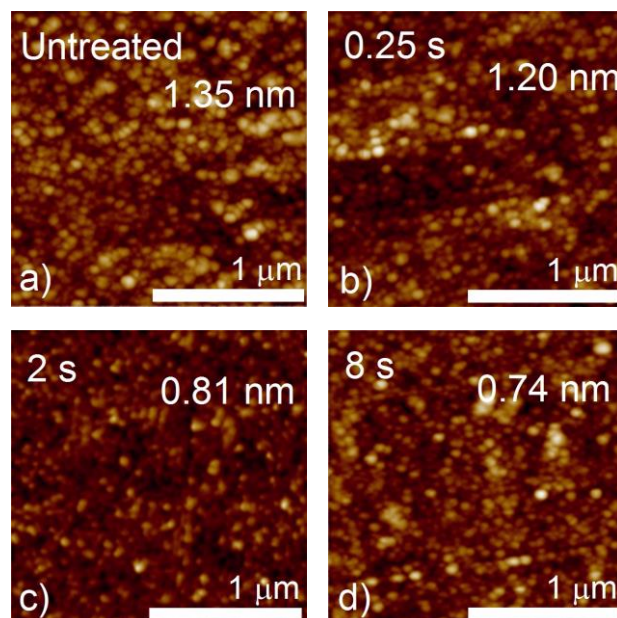
Figure 6. AFM scans of ITO surfaces treated in plasma for a) 0 s, b) 0.25 s c) 2 s and d) 8 s. RMS roughness values are embedded in the AFM scans.

3.5. Wetting properties of TiO₂ ink ITO/PET.

The calculated polar and dispersive components of the surface energy discussed in section 3.2 were further employed to plot wetting envelope diagrams. These conveniently illustrate the degree of wetting for a particular liquid-solid combination and have been proven useful for the rational evaluation of ink/substrate compatibility and process optimization [56]. The envelopes are obtained by calculating the hypothetical polar and dispersive components of the free surface energy which would result in a contact-angle value of 0° (or any other desired value). By plotting the polar fraction against the dispersive fraction, an enclosed area indicating complete (for CA = 0°) or partial (for CA >0°) wetting was obtained. It was observed that wetting was highly irregular for an untreated ITO surface (**Figure 7a**), resulting in development of an "orange-peel texture", an undesirable phenomenon all too familiar in many wet-coating techniques. The corresponding wetting envelope clearly illustrates the physical reason for such behaviour, in that the contact angle of the ink exceeds 30°. However, plasma treatment quickly increases the surface energy in such a way that the 0° envelope encompasses the position of the ink and results in much improved (**Figure 7b**) and almost perfect (**Figure 7c**) wetting. With prolonged plasma treatment, surface energy saturation is observed (**Figure 4a**), and the wetting envelopes do not expand farther (**Figure 7d**). However, further changes in the ink wetting behaviour were observed. A banding pattern developed, originating from the sequential nature of the printing process, in which the 16-nozzle inkjet print-head builds the layer from the individual 16-droplet-wide bands. While in previous cases (**Figures 7b and c**) the printed bands merge to form a more homogeneous layer, in the final case the printed liquid retracts and the width of the band is reduced, preventing it merging with the previous bands. This phenomenon surely bears a relation to excessive plasma treatment, but no immediate explanation is provided by Owens-Wendt wetting theory.
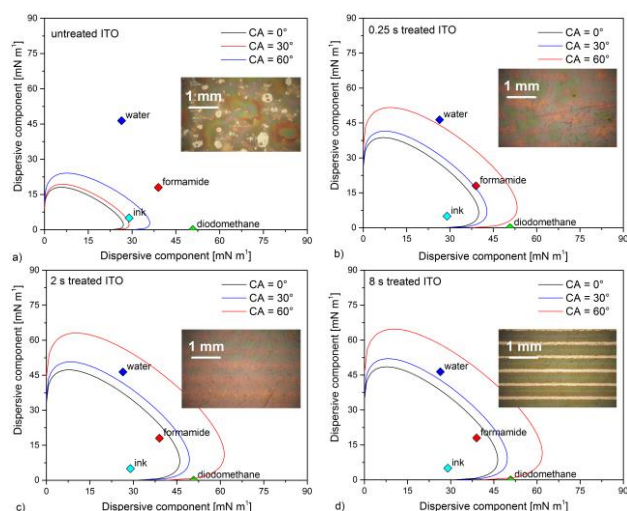

Figure 7. Wetting envelope diagrams for a) untreated ITO and ITO treated in plasma for b) 0.25 s; c) 2 s; and d) 8 s.

The reported results clearly indicate that plasma treatment for 2 s delivers optimum wetting behaviour. **Figure 8** shows titania photoanodes printed onto ITO/PET

flexible foil pre-treated in plasma for 2 s. The photoanode has a macroscopically homogeneous, white surface.

Figure 8. TiO₂/SiO₂ hybrid nanocomposite flexible photoanodes inkjet-printed onto ITO/PET foil.

3.6. Electrochemical activity of TiO₂ ink.

After inkjet printing on 2-s plasma-treated ITO/PET, the flexible TiO₂/SiO₂ films were further mineralized in plasma for 1 – 64 s in order to remove the methyl groups in Si–CH₃ and transform the semiorganic binder into fully mineralized amorphous SiO₂. The mineralization process had no negative effect on the surface morphology of the mesoporous coating; electron microscopy revealed no damage [40]. Chronoamperometric measurements appear in **Figure 9,** and it is apparent that plasma mineralization led to a remarkable increase in the magnitude of the photocurrents generated. Whereas untreated TiO₂/SiO₂ exhibited small and/or negligible current at approx. 1 μA/cm², plasma mineralization resulted in an increase in current to over 15 μA/cm² for TiO₂/SiO₂ mineralized for 64 s. The results presented herein are different to those reported in the authors' previous work [40]. Further, the plasma mineralization herein resulted in significantly lower photo-currents and an increase in dark currents was observed. The difference between total current values may be explained by differences in resistivity between the flexible ITO surfaces used here and the previously-employed rigid FTO glass substrate. Whereas the surface resistivity of flexible ITO was 60 Ω/sq, the surface resistivity of the FTO was 10 Ω/sq, which is 6 times lower and presented currents were approx. 3 – 4 times lower that those reported previously for FTO. The difference is further illustrated in **Figure S5** in Supplementary material along

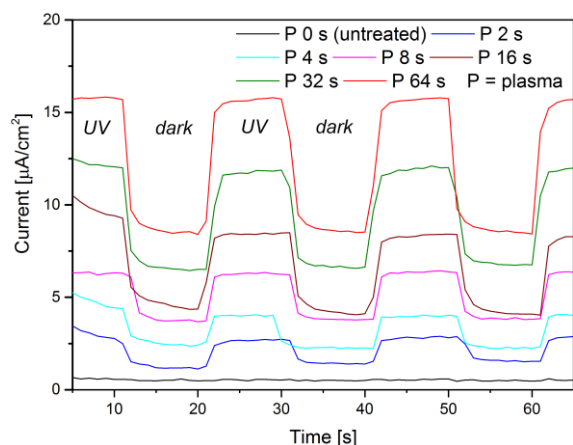with total concentration of carbon in TiO_2/SiO_2 as detected by XPS.

Figure 9. Chronoamperometric records at a period of 10 s for TiO_2 mineralized in plasma for 1 – 64 s. The recorded curves are vertically offset for purposes of clarity.

The individual values of photo- and dark current and total generated current are plotted in **Figure 10.** The plasma mineralization led clearly to an increase in dark current. However, this increase was not evenly graduated and reached saturation at 3 $\mu A/cm^2$ for plasma mineralization at 2 s. The reported increase in dark current may be attributed to plasma pre-treatment of the ITO surface. The FTO surface in [40] was not pre-treated in plasma because wetting of TiO_2/SiO_2 ink on FTO was already sufficient to produce coating of high homogeneity. The increase in photocurrent was progressive and in line with previous reported measurements on plasma-induced binder mineralization. Whereas the untreated surface gave zero photocurrents, the photocurrent in TiO_2/SiO_2 coating mineralized for 64 s showed photocurrent at 7 $\mu A/cm^2$. The total generated current reached 10 $\mu A/cm^2$ after plasma mineralization for 64 s. Therefore both plasma pre-treatment and plasma post-treatment, i.e. mineralization, are important for high photocurrents in TiO_2/SiO_2 mesoporous photoanodes.
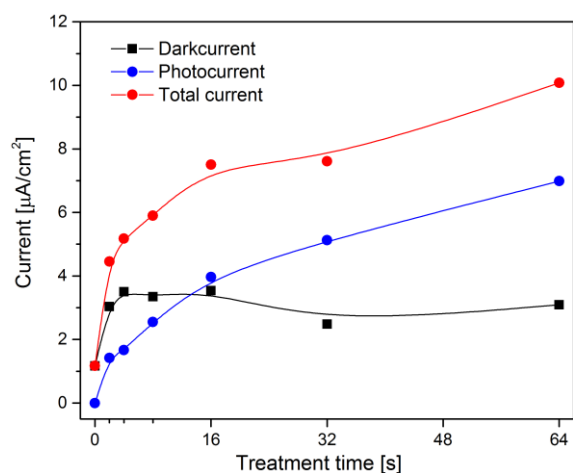

Figure 10. Single dark- and photo-current records including total current (all extracted from Fig. 9) showing saturated increase in dark current and graduated increase in photo- and total current for photoanodes mineralized in plasma for 2 – 64 s.

3.7. Efficiency of plasma treatment.

The energy efficiency demonstrated by atmospheric diffuse coplanar surface barrier discharge plasma was higher than other reported atmospheric plasmas, such as those generated by plasma jets. The atmospheric plasma He/O_2 plasma jet, used for FTO surface activation prior to CdS deposition for photovoltaic application [36], operated at an energy efficiency of 16 J/cm^2, whereas the DCSBD plasma reported herein operated at an energy efficiency of under 5 J/cm^2, and moreover in low-cost ambient air. Although He/O_2 DBD plasma jet [36] pre-treatment of an FTO surface led to swift reduction of carbon contamination and surface activation, its capacity for removal of larger particles was negligible and a wet cleaning process was still required [36]. Generation of active surface plasma in DCSBD also leads to etching that eliminates particles and larger contaminants. In contrast with other plasma treatments that utilize active plasma rather than remote plasma [57], the temperature of DCSBD may be as low as 70 °C and therefore the etching is a plasma-chemical, rather than a thermal process, and does not lead to surface damage (e.g. pin-holing). Very recently, Seidelmann reported on roll-to-roll atmospheric pressure plasma treatment of polymeric films using dielectric barrier discharge [58]. The discharge operated at approx. 10 J/cm^2 (power density 0.7 $W.cm^{-2}$, treatment speed 37 $cm.s^{-1}$). However, the stability and diffusivity of the plasma was achieved by means of pure nitrogen and the reactor operated at low pressure.

It is apparent that the high efficiency of the DCSBD plasma arose from its coplanar electrode setup, which facilitated the generation of diffuse and high-energy plasma in practically any working gas.

4. Conclusions

This contribution presents a method for the fabrication of flexible mesoporous TiO_2 photoanodes using cold (70 °C) plasma in ambient air in roll-to-roll configuration. First, ambient air plasma was used to treat the surface of flexible ITO/PET foil. The plasma treatment significantly improved subsequent printing quality and wetting of TiO_2/SiO_2 coatings on ITO/PET foils. In addition to excellent wetting, the work function of the ITO increased significantly with plasma treatment. It should be noted that plasma engineering of the work function can be directly related to charge outcoupling efficiency and subsequently leads to leads to higher open-circuit voltages and improved power conversion efficiency in solar cells [54,59]. A further advantage of atmospheric pressure plasma treatment of ITO surfaces is that it is much faster than low-pressure plasma [60–62], which is also impractical for roll-to-roll applications.

The TiO_2/SiO_2 films were further mineralized using the same plasma setup with longer processing times, up to 64 s. Despite the low temperature of the plasma treatment, it was capable of removing the organic portions of the binder efficiently, while preserving the mesoporous structure of the TiO_2 photoanodes. Subsequently the TiO_2

photoanodes showed a significant increase in generated photocurrent and excellent mechanical stability when printed onto flexible ITO/PET.

The methods presented herein may well provide the foundations for an important step forward towards large-scale, low-cost manufacturing of flexible energy harvesting systems.

Supplementary Material

Supporting Material is available online.

Acknowledgements

References

[1] Bringans R D and Veres J 2016 Challenges and opportunities in flexible electronics *2016 IEEE International Electron Devices Meeting (IEDM)* (IEEE) p 6.4.1-6.4.2

[2] Kamyshny A and Magdassi S 2014 Conductive Nanomaterials for Printed Electronics *Small* **10** 3515–35

[3] Weerasinghe H C, Huang F and Cheng Y-B 2013 Fabrication of flexible dye sensitized solar cells on plastic substrates *Nano Energy* **2** 174–89

[4] Gong J, Liang J and Sumathy K 2012 Review on dye-sensitized solar cells (DSSCs): Fundamental concepts and novel materials *Renewable Sustainable Energy Rev.* **16** 5848–60

[5] Hashmi S G, Özkan M, Halme J, Zakeeruddin S M, Paltakari J, Grätzel M and Lund P D 2016 Dye-sensitized solar cells with inkjet-printed dyes *Energy Environ. Sci.* **9** 2453–62

[6] Gong J, Sumathy K, Qiao Q and Zhou Z 2017 Review on dye-sensitized solar cells (DSSCs): Advanced techniques and research trends *Renewable Sustainable Energy Rev.* **68** 234–46

[7] Grätzel M 2017 The Rise of Highly Efficient and Stable Perovskite Solar Cells *Acc. Chem. Res.* **50** 487–91

[8] Williams S T, Rajagopal A, Chueh C-C and Jen A K-Y 2016 Current Challenges and Prospective Research for Upscaling Hybrid Perovskite Photovoltaics *J. Phys. Chem. Lett.* **7** 811–9

[9] Razza S, Castro-Hermosa S, Di Carlo A and Brown T M 2016 Research Update: Large-area deposition, coating, printing, and processing techniques for the upscaling of perovskite solar cell technology *APL Mater.* **4** 91508

[10] Green M A and Ho-Baillie A W-Y 2017 Perovskite Solar Cells: The Birth of a New Era in Photovoltaics *ACS Energy Lett.* **2** 822–30

[11] Levchuk I, Sillanpää M, Guillard C, Gregori D, Chateau D, Chaput F, Lerouge F and Parola S 2016 Enhanced photocatalytic activity through insertion of plasmonic nanostructures into porous TiO2/SiO2 hybrid composite films *J. Catal.* **342** 117–24

[12] Méndez-Medrano M G, Kowalska E, Lehoux A, Herissan A, Ohtani B, Rau S, Colbeau-Justin C, Rodríguez-López J L and Remita H 2016 Surface Modification of TiO₂ with Au Nanoclusters for Efficient Water Treatment and Hydrogen Generation under Visible Light *J. Phys. Chem. C* **120** 25010–22

[13] Eftekhari A, Babu V J and Ramakrishna S 2017 Photoelectrode nanomaterials for photoelectrochemical water splitting *Int. J. Hydrogen Energy* **42** 11078–109

[14] Priebe J B, Radnik J, Lennox A J J, Pohl M-M, Karnahl M, Hollmann D, Grabow K, Bentrup U, Junge H, Beller M and Brückner A 2015 Solar Hydrogen Production by Plasmonic Au–TiO2 Catalysts: Impact of Synthesis Protocol and TiO2 Phase on Charge Transfer Efficiency and H2 Evolution Rates *ACS Catal.* **5** 2137–48

[15] Li W, Wang F, Liu Y, Wang J, Yang J, Zhang L, Elzatahry A A, Al-Dahyan D, Xia Y and Zhao D 2015 General Strategy to Synthesize Uniform Mesoporous TiO2/Graphene/Mesoporous TiO2 Sandwich-Like Nanosheets for Highly Reversible Lithium Storage *Nano Lett.* **15** 2186–93

[16] Wang W, Liu Y, Sun J and Gao L 2016 Nitrogen and yttrium co-doped mesoporous titania photoanodes applied in DSSCs *J. Alloys Compd.* **659** 15–22

[17] Giordano F, Abate A, Correa Baena J P, Saliba M, Matsui T, Im S H, Zakeeruddin S M, Nazeeruddin M K, Hagfeldt A and Graetzel M 2016 Enhanced electronic properties in mesoporous TiO2 via lithium doping for high-efficiency perovskite solar cells. *Nat. Commun.* **7** 10379

[18] Arnou P, van Hest M F A M, Cooper C S, Malkov A V., Walls J M and Bowers J W 2016 Hydrazine-Free Solution-Deposited CuIn(S,Se)₂ Solar Cells by Spray Deposition of Metal Chalcogenides *ACS Appl. Mater. Interfaces* **8** 11893–7

[19] Supriyanto A, Furqoni L, Nurosyid F, Hidayat J and Suryana R 2016 Effect of sintering temperatures and screen printing types on TiO2 layers in DSSC applications *AIP Conf. Proc.* **1717** 40001

[20] Vak D, Weerasinghe H, Ramamurthy J, Subbiah J, Brown M and Jones D J 2016 Reverse gravure coating for roll-to-roll production of organic photovoltaics *Sol. Energy Mater. Sol. Cells* **149** 154–61

[21] Homenick C M, James R, Lopinski G P, Dunford J, Sun J, Park H, Jung Y, Cho G and Malenfant P R L 2016 Fully Printed and Encapsulated SWCNT-Based Thin Film Transistors via a Combination of R2R Gravure and Inkjet Printing *ACS Appl. Mater. Interfaces* **8** 27900–10

[22] Alamán J, Alicante R, Peña J and Sánchez-Somolinos C 2016 Inkjet Printing of Functional Materials for Optical and Photonic Applications *Materials (Basel).* **9** 910

[23] Mariani P, Vesce L and Di Carlo A 2015 The role of printing techniques for large-area dye sensitized solar cells *Semicond. Sci. Technol.* **30** 104003

[24] Hu Q, Wu H, Sun J, Yan D, Gao Y and Yang J 2016 Large-area perovskite nanowire arrays fabricated by large-scale roll-to-roll micro-gravure printing and doctor blading *Nanoscale* **8** 5350–7

[25] Chou C-Y, Chang H, Liu H-W, Yang Y-J, Hsu C-C, Cheng I-C and Chen J-Z 2015 Atmospheric-pressure-plasma-jet processed nanoporous TiO2 photoanodes and Pt counter-electrodes for dye-sensitized solar cells *RSC Adv.* **5** 45662–7

[26] Kim H and Hwang T 2014 Effect of titanium isopropoxide addition in low-temperature cured TiO2 photoanode for a flexible DSSC *J. Sol-Gel Sci. Technol.* **72** 67–73

[27] Jiang Y F, Chen Y Y, Zhang B and Feng Y Q 2016 N, La Co-Doped TiO2 for Use in Low-Temperature-Based Dye-Sensitized Solar Cells *J. Electrochem. Soc.* **163** F1133–8

[28] Zardetto V, Brown T M, Reale A and Di Carlo A 2011 Substrates for flexible electronics: A practical investigation on the electrical, film flexibility, optical, temperature, and solvent resistance properties *J. Polym. Sci. Part B Polym. Phys.* **49** 638–48

[29] Yasin A, Guo F and Demopoulos G P 2016 Aqueous, Screen-Printable Paste for Fabrication of Mesoporous Composite Anatase–Rutile TiO₂ Nanoparticle Thin Films for (Photo)electrochemical Devices *ACS Sustain. Chem. Eng.* **4** 2173–81

[30] Li R, Zhao Y, Hou R, Ren X, Yuan S, Lou Y, Wang Z, Li D and Shi L 2016 Enhancement of power conversion efficiency of dye sensitized solar cells by modifying mesoporous TiO2 photoanode with Al-doped TiO2 layer *J. Photochem. Photobiol. A Chem.* **319–320** 62–9

[31] Wang Y, Yuan Q, Yin G, Zhang Y, Zhang Y, Li Y, Li J, Wang T and Ma S 2016 Synthesis of Mixed-Phase TiO2 Nanopowders Using Atmospheric Pressure Plasma Jet Driven by Dual-Frequency Power Sources *Plasma Chem. Plasma Process.* **36** 1471–84

[32] Chou W-C and Liu W-J 2016 Study of dye sensitized solar cell application of TiO2 films by atmospheric pressure plasma deposition method *2016 International Conference on Electronics Packaging (ICEP)* (IEEE) pp 664–8

[33] Islam S Z, Reed A, Wanninayake N, Kim D Y and Rankin S E 2016 Remarkable Enhancement of Photocatalytic Water Oxidation in N2/Ar Plasma Treated, Mesoporous TiO2 Films *J. Phys. Chem. C* **120** 14069–81

[34] Islam S Z, Reed A, Kim D Y and Rankin S E 2016 N2/Ar plasma

induced doping of ordered mesoporous TiO2 thin films for visible light active photocatalysis *Microporous Mesoporous Mater.* **220** 120–8

[35] Mariotti D, Belmonte T, Benedikt J, Velusamy T, Jain G and Švrček V 2016 Low-Temperature Atmospheric Pressure Plasma Processes for "Green" Third Generation Photovoltaics *Plasma Process. Polym.* **13** 70–90

[36] Lisco F, Shaw A, Wright A, Walls J M and Iza F 2017 Atmospheric-pressure plasma surface activation for solution processed photovoltaic devices *Sol. Energy* **146** 287–97

[37] Lisco F, Shaw A, Wright A, Iza F and Walls J M 2016 Surface activation of rigid and flexible substrates for thin film photovoltaics using atmospheric pressure plasma *2016 IEEE 43rd Photovoltaic Specialists Conference (PVSC)* (IEEE) pp 2204–9

[38] Griffith M J, Cooling N A, Vaughan B, Elkington D C, Hart A S, Lyons A G, Quereshi S, Belcher W J and Dastoor P C 2016 Combining Printing, Coating, and Vacuum Deposition on the Roll-to-Roll Scale: A Hybrid Organic Photovoltaics Fabrication *IEEE J. Sel. Top. Quantum Electron.* **22** 112–25

[39] Søndergaard R R, Hösel M and Krebs F C 2013 Roll-to-Roll fabrication of large area functional organic materials *J. Polym. Sci. Part B Polym. Phys.* **51** 16–34

[40] Homola T, Dzik P, Veselý M, Kelar J, Černák M and Weiter M 2016 Fast and low-temperature (70 °C) mineralization of inkjet printed mesoporous TiO2 photoanodes using ambient air plasma *ACS Appl. Mater. Interfaces* **8** 33562–71

[41] Medvecká V, Kováčik D, Zahoranová A, Stupavská M and Černák M 2016 Atmospheric pressure plasma assisted calcination of organometallic fibers *Mater. Lett.* **162** 79–82

[42] Medvecká V, Kováčik D, Tučeková Z, Zahoranová A and Černák M 2016 Atmospheric pressure plasma assisted calcination of composite submicron fibers ed N Gherardi, E Marotta and C Paradisi *Eur. Phys. J. Appl. Phys.* **75** 24715

[43] Mudra E, Streckova M, Pavlinak D, Medvecka V, Kovacik D, Kovalcikova A, Zubko P, Girman V, Dankova Z, Koval V and Duzsa J 2016 Development of Al2O3 electrospun fibers prepared by conventional sintering method or plasma assisted surface calcination *Appl. Surf. Sci.*

[44] Homola T, Matoušek J, Kormunda M, Wu L Y L and Černák M 2013 Plasma treatment of glass surfaces using diffuse coplanar surface barrier discharge in ambient air *Plasma Chem. Plasma Process.* **33** 881–94

[45] Grégori D, Benchenaa I, Chaput F, Thérias S, Gardette J-L, Léonard D, Guillard C and Parola S 2014 Mechanically stable and photocatalytically active TiO2/SiO2 hybrid films on flexible organic substrates *J. Mater. Chem. A* **2** 20096–104

[46] Owens D K and Wendt R C 1969 Estimation of the surface free energy of polymers *J. Appl. Polym. Sci.* **13** 1741–7

[47] Dzik P, Veselý M and Neumann-Spallart M 2016 Inkjet Printed Interdigitated Conductivity Cells with Low Cell Constant *ECS J. Solid State Sci. Technol.* **5** P412–8

[48] Huang P-R, He Y, Cao C and Lu Z-H 2013 The origin of the high work function of chlorinated indium tin oxide *NPG Asia Mater.* **5** e57

[49] Homola T, Matoušek J, Medvecká V, Zahoranová A, Kormunda M, Kováčik D and Černák M 2012 Atmospheric pressure diffuse plasma in ambient air for ITO surface cleaning *Appl. Surf. Sci.* **258** 7135–9

[50] Borcia C, Punga I L and Borcia G 2014 Surface properties and hydrophobic recovery of polymers treated by atmospheric-pressure plasma *Appl. Surf. Sci.* **317** 103–10

[51] Van Deynse A, Cools P, Leys C, Morent R and De Geyter N 2014 Influence of ambient conditions on the aging behavior of plasma-treated polyethylene surfaces *Surf. Coatings Technol.* **258** 359–67

[52] Tang C G, Ang M C Y, Choo K-K, Keerthi V, Tan J-K, Syafiqah M N, Kugler T, Burroughes J H, Png R-Q, Chua L-L and Ho P K H 2016 Doped polymer semiconductors with ultrahigh and ultralow work functions for ohmic contacts *Nature* **539** 536–40

[53] Kahn A 2016 Fermi level, work function and vacuum level *Mater. Horiz.* **3** 7–10

[54] Kuo F-L, Li Y, Solomon M, Du J and Shepherd N D 2012 Workfunction tuning of zinc oxide films by argon sputtering and oxygen plasma: an experimental and computational study *J. Phys. D. Appl. Phys.* **45** 65301

[55] Sun W, Li Y, Jha J K, Shepherd N D and Du J 2015 Effect of surface adsorption and non-stoichiometry on the workfunction of ZnO surfaces: A first principles study *J. Appl. Phys.* **117** 165304

[56] Dzik P, Veselý M and Neumann-Spallart M 2016 Inkjet Printed Interdigitated Conductivity Cells with Low Cell Constant *ECS J. Solid State Sci. Technol.* **5** P412–8

[57] Homola T, Wu L Y L and Černák M 2014 Atmospheric Plasma Surface Activation of Poly(Ethylene Terephthalate) Film for Roll-To-Roll Application of Transparent Conductive Coating *J. Adhes.* **90** 296–309

[58] Seidelmann L, Bradley J, Ratova M, Hewitt J, Moffat J and Kelly P 2017 Reel-to-Reel Atmospheric Pressure Dielectric Barrier Discharge (DBD) Plasma Treatment of Polypropylene Films *Appl. Sci.* **7** 337

[59] Hinckley A C, Wang C, Pfattner R, Kong D, Zhou Y, Ecker B, Gao Y and Bao Z 2016 Investigation of a Solution-Processable, Nonspecific Surface Modifier for Low Cost, High Work Function Electrodes *ACS Appl. Mater. Interfaces* **8** 19658–64

[60] Yang L, Guo S, Yang Q, Zhu Y, Dai B, Yu H, Lei P, Han J, Hou Y and Zhu J 2015 Improved work function of preferentially oriented indium oxide films induced by the plasma exposure technique *Electron. Mater. Lett.* **11** 938–43

[61] Ke J-C, Wang Y-H, Chen K-L and Huang C-J 2016 Effect of organic solar cells using various power O2 plasma treatments on the indium tin oxide substrate *J. Colloid Interface Sci.* **465** 311–5

[62] Vunnam S, Ankireddy K, Kellar J and Cross W 2013 Surface modification of indium tin oxide for direct writing of silver nanoparticulate ink micropatterns *Thin Solid Films* **531** 294–301